Cobalt Metal−Organic Frameworks Incorporating Redox-Active Tetrathiafulvalene Ligand: Structures and Effect of LLCT within MOF on Photoelectrochemical Properties

Miao Jiang, Yi-Gang Weng, Zi-Yao Zhou, Chen-Yi Ge, Qin-Yu Zhu,* and Jie Dai*

College of Chemistry, Chemical Engineering and Materials Science, Soochow University, Suzhou 215123, P. R. China

1. Characterizations and measurements

2. Figures

Figure S1. The experimental powder XRD patterns and the simulated pattern from the crystal data of compounds **1**–**3**.

Figure S2. 1D Co4–Co5–Co6 chain structure bridged by carboxylate groups of L in **1**.

Figure S3. 2D network of **1** indicating the arrangement of the six cobalt ions linked by carboxylate groups of L and bpe. Hydrogen atoms and ligand L except those related coordination atoms are omitted for clarity.

Figure S4. The sketch maps of the planes of parts of bpe and L in **1**.

Figure S5. Structures of Co_5 clusters in this work and previously reports.

Figure S6. Stick representation of the cluster chain in **2** along the *a* axis showing that TTF is located evenly in the four directions of the chain. bpe is omitted except the coordinated nitrogen atoms for clarity.

Figure S7. A part of the packing diagram of **2** showing the π···π interactions between the TTF moiety and bpe molecule.

Figure S8. (a) An infinite –Co–O–C–O–Co– 1-D chain along the *b* axis constructed by carboxylate bridges of **3.** bpa except the coordinated nitrogen atoms and all hydrogen atoms are omitted for clarity; (b) 2-D network structure of **3**. L except the coordinated carboxylate groups and all hydrogen atoms are omitted for clarity.

Figure S9. Solid-state ESR spectra of **1** and **2** recorded at 120 K.

Figure S10. (a) CV curves of **1** at different scan rates. (b) The integrated area of the CV curves and the specific capacitances of **1** at different scan rates. (c) GCD curves of **1** at different current intensities. (d) Variation of specific capacitance of **1** with

applied currents.

Figure S11. (a) CV curves of **2** at different scan rates. (b) The integrated area of the CV curves and the specific capacitances of **2** at different scan rates. (c) GCD curves of **2** at different current intensities. (d) Variation of specific capacitance of **2** with applied currents.

Figure S12. Curves of the peak currents vs the square roots of scan rates of **1**, **2**, and **3** for CV measurements.

Figure S13. The specific capacitances of **1**, **2**, and **3** at different scan rates.

3. Tables

Table S1. The mean deviations from the planes of the TTF moiety and bpe, the dihedral angles and the distances between least-squares planes in **1** and **2**.

Table S2. Comparison of Csp values of various Co-MOF materials.

Table S3. Crystal data and structural refinement parameters for compounds **1**–**3**.

4. Equations

1. Characterizations and Measurements

General Remarks.

The sodium salt of dimethylthio-tetrathiafulvalene–bicarboxylate (Na_2L) was prepared according to the literature.[1] All analytically pure reagents were purchased commercially and used without further purification. Elemental analyses (C, H, and N) were performed using a VARIDEL III elemental analyzer. Solid-state room-temperature optical diffuse reflectance spectra of the microcrystal samples were obtained with a Shimadzu UV-2600 spectrophotometer using $BaSO_4$ as a standard reference. Powder X-ray diffraction (PXRD) data were obtained using a D/MAX-3C X-ray diffraction meter with CuKα (λ = 1.5406 Å) radiation. Cyclic voltammetry (CV) experiments were performed on a CHI650 electrochemistry workstation in a three-electrode system with a Pt plate working electrode, a saturated calomel electrode (SCE) as reference electrode, and Pt wire as the auxiliary electrode. Electron spin resonance (ESR) spectra were carried out at 120 K and obtained using a Bruker ER-420 spectrometer with a 100 kHz magnetic field in X band.

X-ray Crystallographic Study.

The crystal data were collected on a Bruker APEX-II CCD diffractometer for **1** and a Rigaku Mercury CCD diffractometer for **2** and **3** equipped with graphite monochromated Mo Kα (λ = 0.71075 Å) radiation were used to carry out the measurements at 223 K. An absorption correction (multiscan) was applied for all these compounds. The structures were solved by direct methods using SHELXS-16 program and the refinements were performed against F^2 using SHELXL-16.[2] Detailed crystal data and structural refinement parameters are listed in Table S3 in the Supporting Information.

Electrode Preparation and Photocurrent Measurement.

The photoelectrodes of the compounds were prepared by powder coating method. As a typical procedure, the crystals of compounds (0.005 mmol) were ground and pressed uniformly on the ITO glass (1.0×1.0 cm, 8 Ω/□). A 150 W high–pressure xenon lamp, located 20 cm away from the surface of the ITO electrode, was employed

as a full-wavelength light source. The photocurrent experiments were performed at room temperature on a CHI660E electrochemistry workstation in a three-electrode system, with the sample coated ITO glass as the working electrode mounted on the window with an area of 0.50 cm^2, a Pt wire as auxiliary electrode and a saturated calomel electrode (SCE) as reference electrode. The supporting electrolyte solution was a 0.1 $mol \cdot L^{-1}$ sodium sulfate aqueous solution. The lamp was kept on continuously, and a manual shutter was used to block exposure of the sample to the light. The sample was typically irradiated at intervals of 20 s.

Fabrication of the working electrodes and electrochemical measurements.

The working electrodes were obtained with the following procedure. The compounds as active materials, acetylene black, and a poly(vinylene fluoride) (PVDF) emulsion, were mixed in ethanol at a weight ratio of 75 : 15 : 10, and dispersed by ultrasonic treatment for 10 min. The slurry was coated on a nickel foam (1.0 × 1.0 cm^2) current collector and then pressed and dried under vacuum at 60 °C for 12 h. The mass of the active loading on the nickel foam was ~3 mg. The electrochemical properties of the active material were tested using a CHI660E electrochemical workstation by a conventional three-electrode system with a calomel reference electrode and a platinum counter electrode. The average specific capacitances of the electrodes were calculated based on the CV curves and the discharge curves, respectively. All of the electrochemical measurements were performed in a 6.0 M KOH solution at room temperature.

References

(1) (a) McCullough, R. D.; Petruska, M. A.; Belot, J. A. *Tetrahedron* **1999**, *55*, 9979–9998. (b) Hudhomme, P.; Moustarder, S. L.; Durand, C.; Gallego-Planas, N.; Mercier, N.; Blanchard, P.; Levillain, E.; Allain, M.; Gorgues, A.; Riou, A. *Chem. Eur. J*. **2001**, *7*, 5070–5083.

(2) (a) Sheldrick, G. M. *SHELXS-97*, Program for structure solution; Universität of Göttingen, Göttingen, Germany, **1999**. (b) Sheldrick, G. M. Crystal structure refinement with SHELXL. *Acta Crystallogr., Sect. C: Struct. Chem.* **2015**, *71*, 3−8.

2. Figures

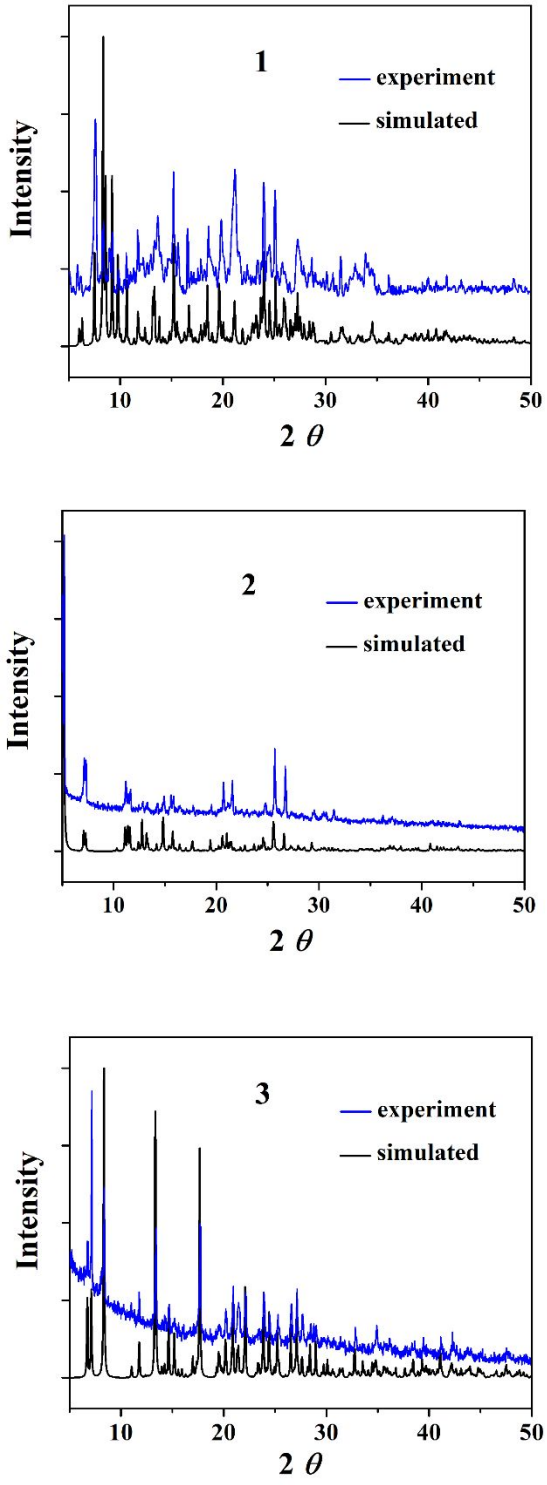

Figure S1. The experimental powder XRD patterns and the simulated pattern from the crystal data of compounds **1**–**3**.

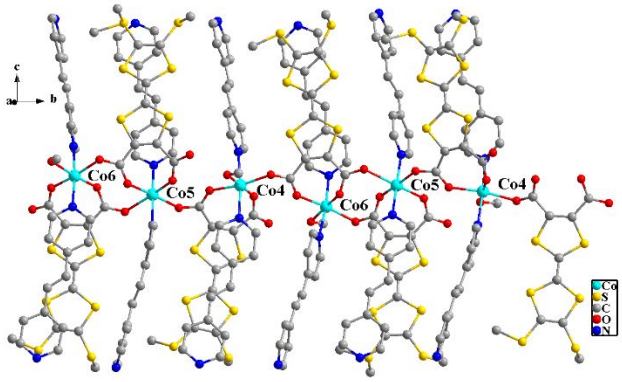

Figure S2. 1D Co4–Co5–Co6 chain structure bridged by carboxylate groups of L in **1**.

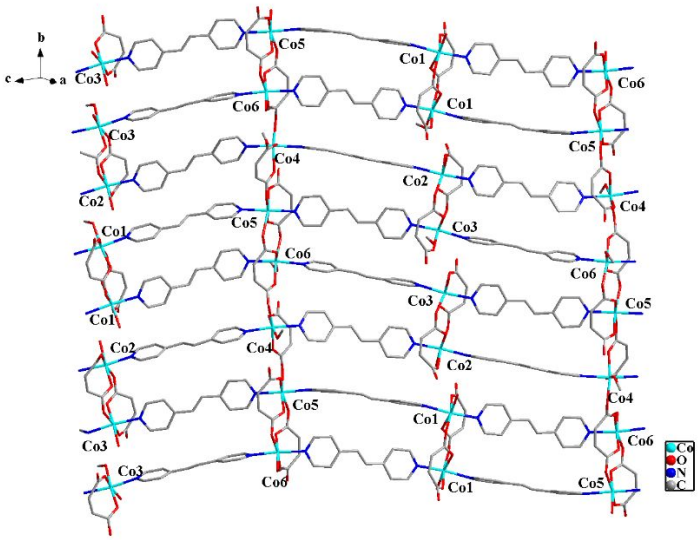

Figure S3. 2D network of **1** indicating the arrangement of the six cobalt ions linked by carboxylate groups of L and bpe. Hydrogen atoms and ligand L except those related coordination atoms are omitted for clarity.

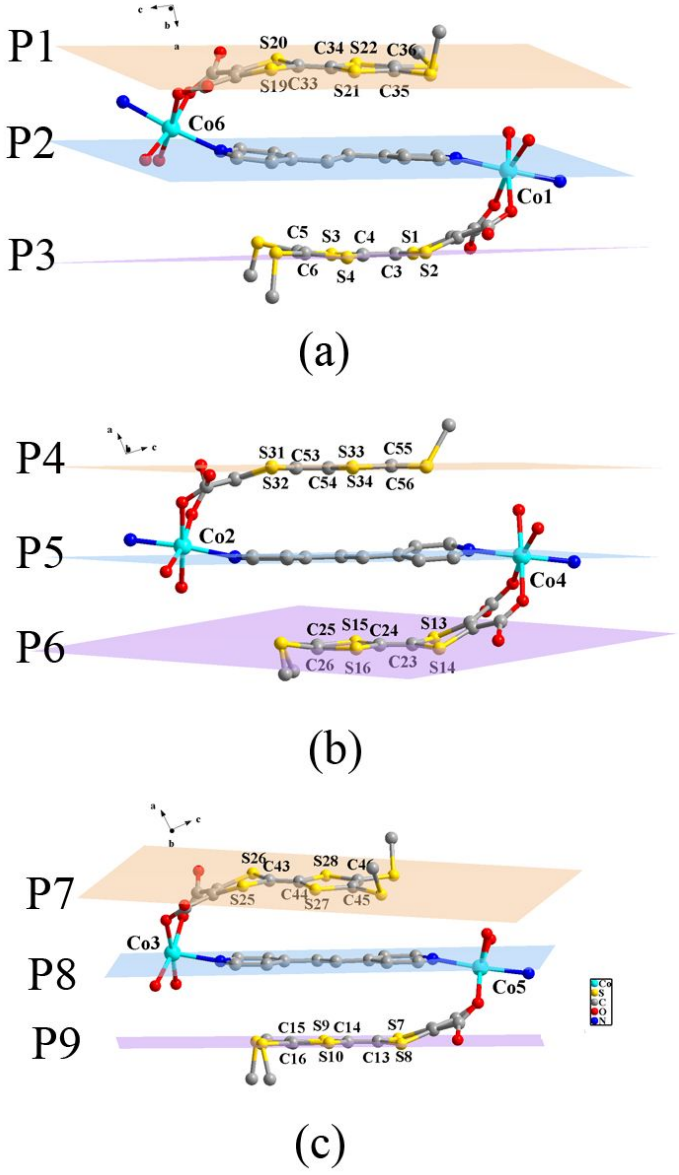

Figure S4. The sketch maps of the planes of parts of L and bpe in **1**.

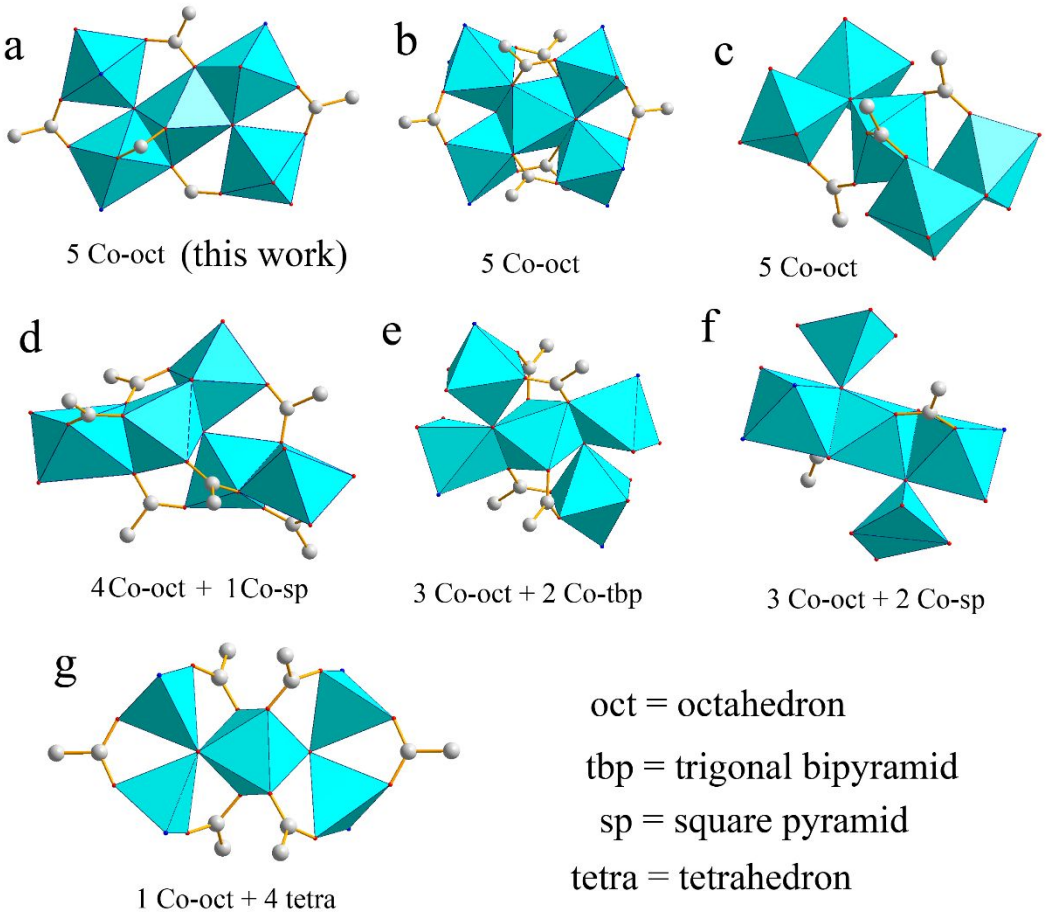

Figure S5. Structures of Co_5 clusters in this work and previously reports.

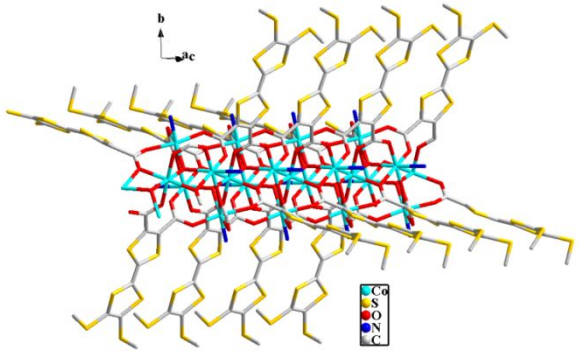

Figure S6. Stick representation of the cluster chain in **2** along the *a* axis showing that TTF is located evenly in the four directions of the chain. bpe is omitted except the coordinated nitrogen atoms for clarity.

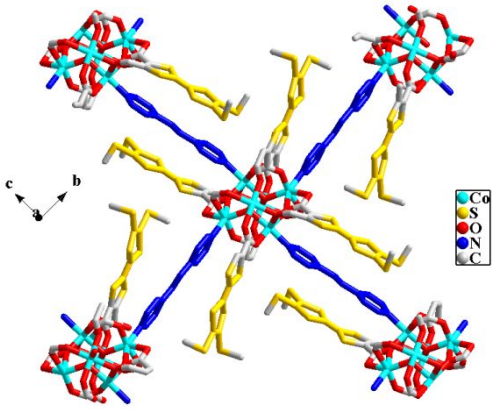

Figure S7. A part of the packing diagram of **2** showing the π···π interactions between the TTF moiety and bpe molecule.

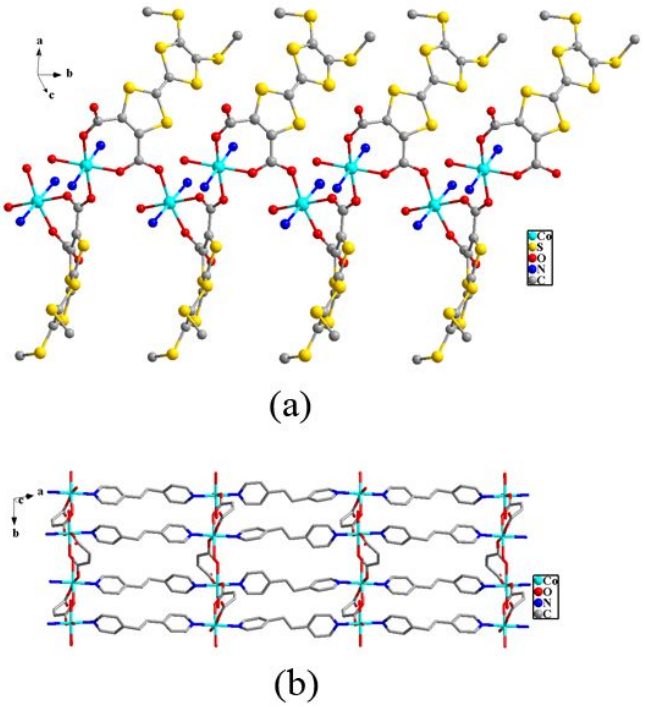

Figure S8. (a) An infinite –Co–O–C–O–Co– 1-D chain along the *b* axis constructed by carboxylate bridges of **3.** bpa except the coordinated nitrogen atoms and all hydrogen atoms are omitted for clarity; (b) 2-D network structure of **3**. L except the coordinated carboxylate groups and all hydrogen atoms are omitted for clarity.

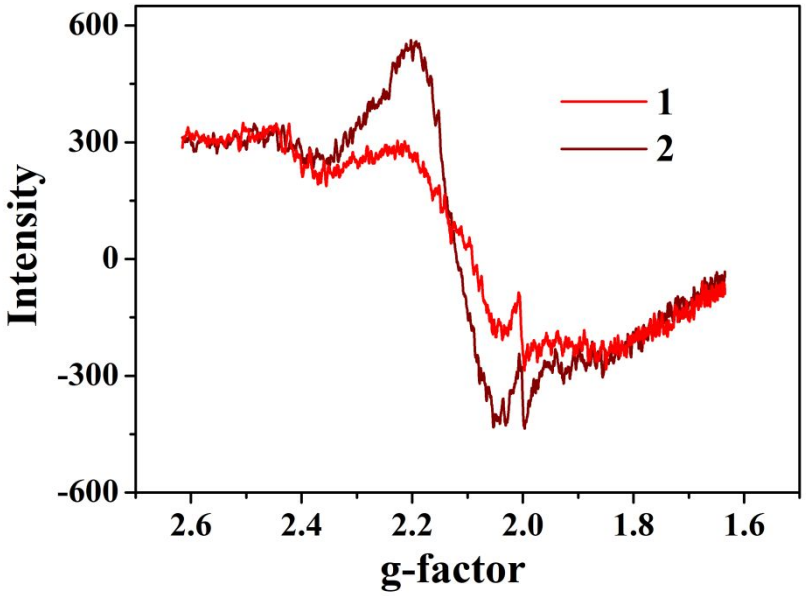

Figure S9. Solid-state ESR spectra of **1** and **2** recorded at 120 K.

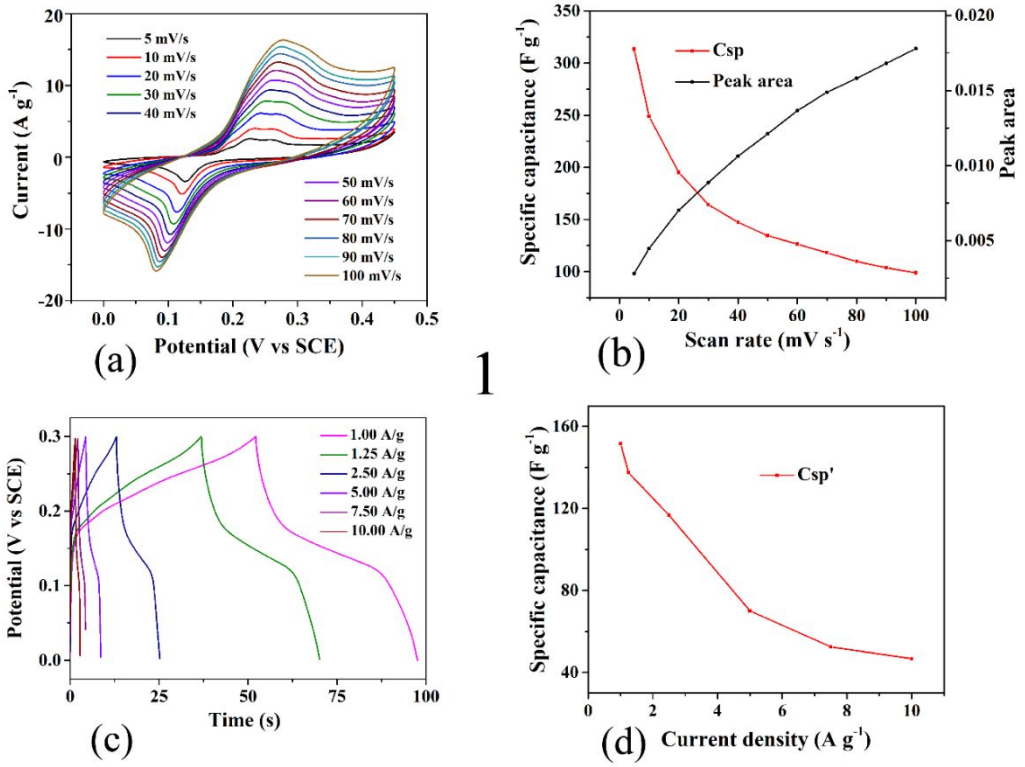

Figure S10. (a) CV curves of **1** at different scan rates. (b) The integrated area of the CV curves and the specific capacitances of **1** at different scan rates. (c) GCD curves of **1** at different current intensities. (d) Variation of specific capacitance of **1** with applied currents.

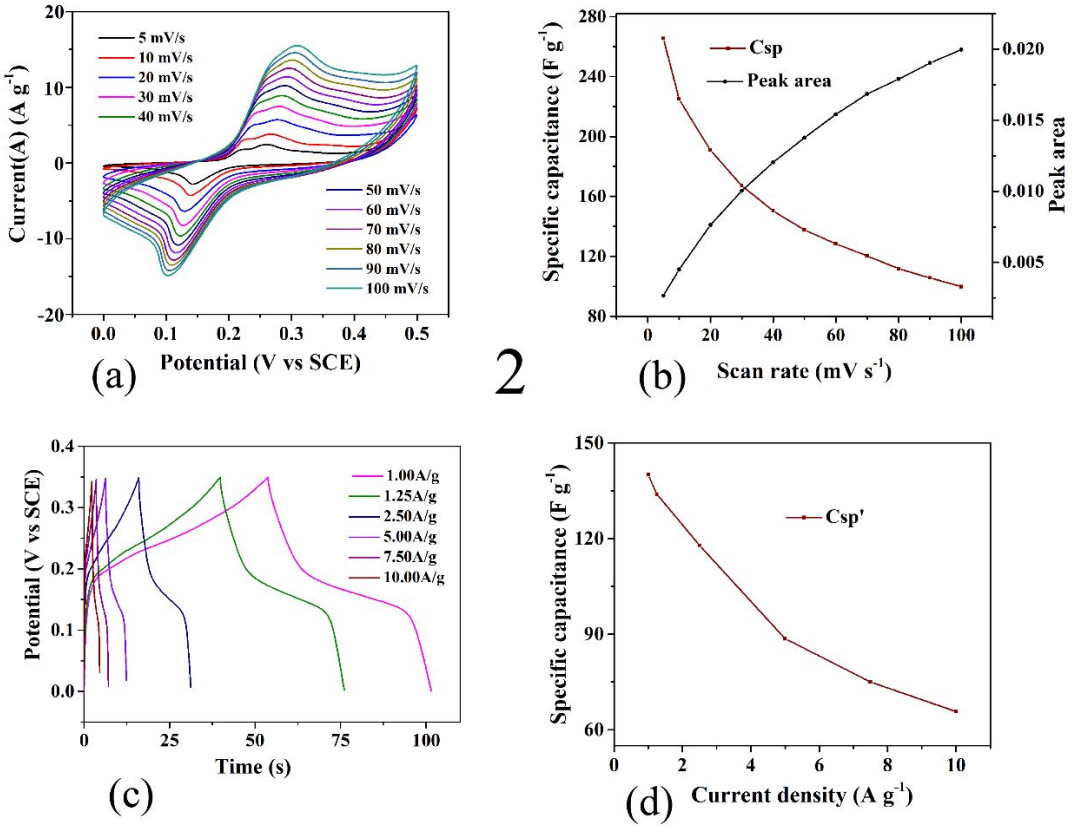

Figure S11. (a) CV curves of **2** at different scan rates. (b) The integrated area of the CV curves and the specific capacitances of **2** at different scan rates. (c) GCD curves of **2** at different current intensities. (d) Variation of specific capacitance of **2** with applied currents.

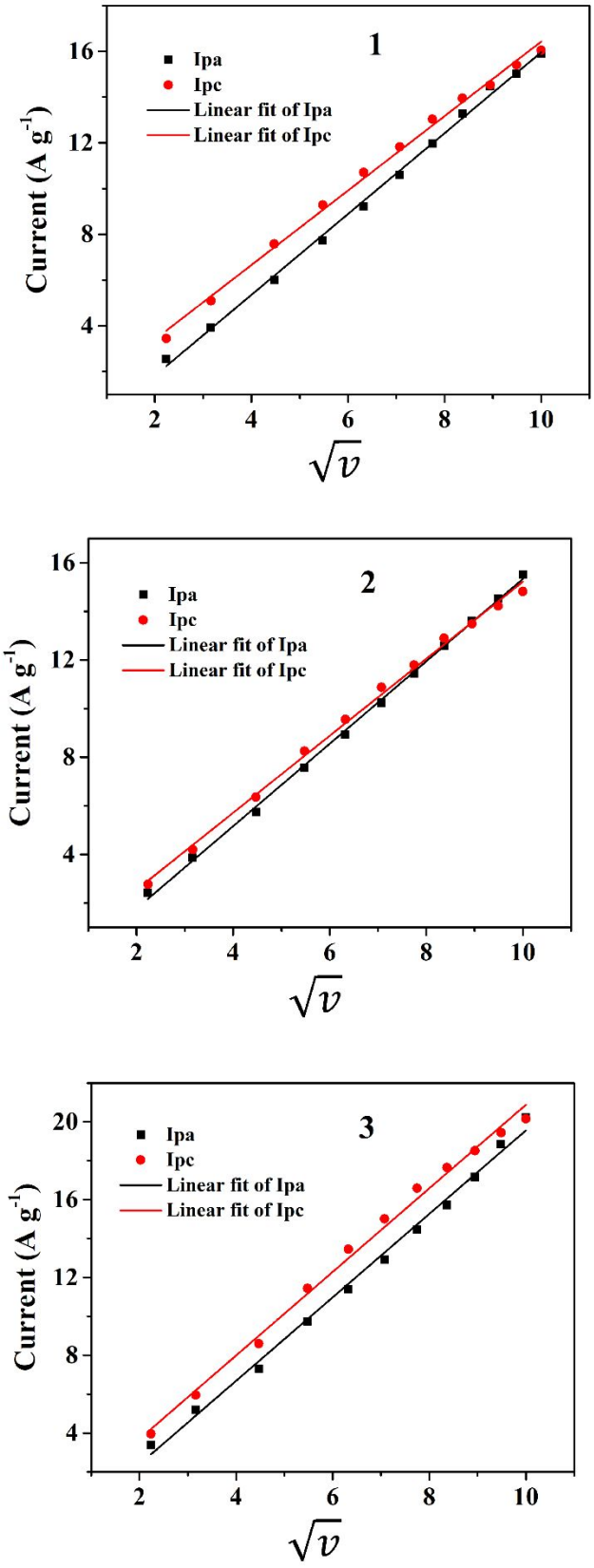

Figure S12. Curves of the peak currents vs the square roots of scan rates of **1**, **2**, and **3** for CV measurements.

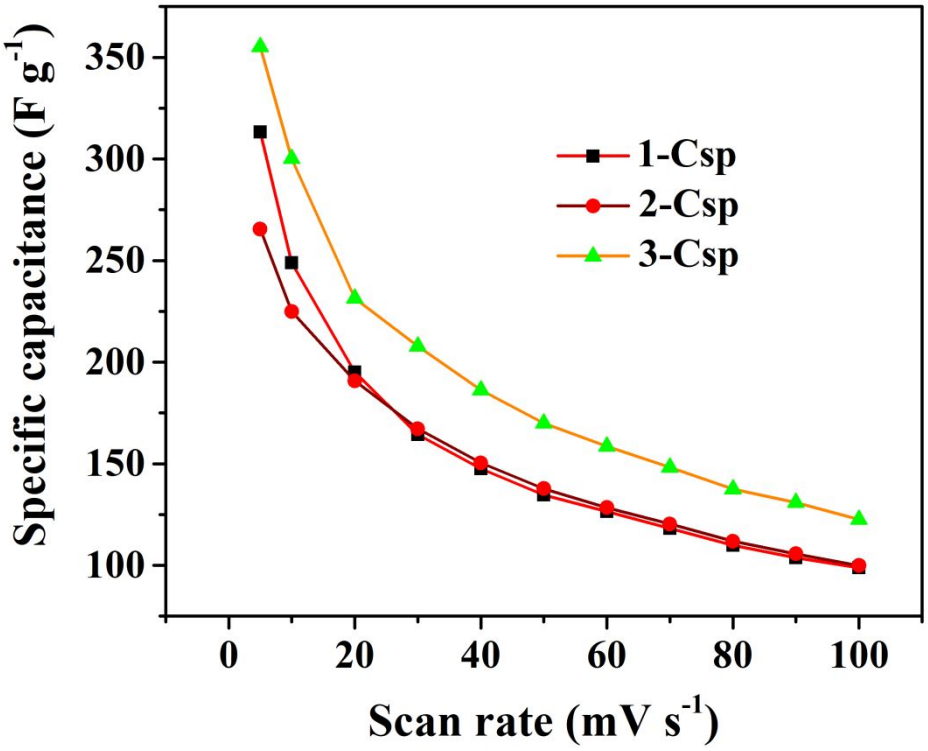

Figure S13. The specific capacitances of **1**, **2**, and **3** at different scan rates.

Table S1. The mean deviations (Å) from the plane of the TTF moiety and of bpe, the dihedral angles (º) and the distances (Å) between least-squares planes in **1** and **2**.

		mean deviation(Å)		**dihedral angle**(º)	**distance between planes**(Å)	
1	P1	0.0233(0.0057)	P1^P2	0.667(131)	P1–P2	3.70
	P2	0.0701(0.0086)	P3^P2	6.545(136)	P3–P2	3.94
	P3	0.0614(0.0064)	P1^P3	7.212(62)		
	P4	0.0230(0.0066)	P4^P5	0.575(205)	P4–P5	3.62
	P5	0.0148(0.0092)	P6^P5	8.427(223)	P6–P5	3.58
	P6	0.0281(0.0076)	P4^P6	7.959(77)		
	P7	0.0121(0.0066)	P7^P8	5.623(151)	P7–P8	3.53
	P8	0.0193(0.0084)	P9^P8	2.941(138)	P9–P8	3.56
	P9	0.0251(0.0066)	P7^P9	7.953(69)		
2	P1	0.0288(0.0100)		2.037(18)		3.63
	P2	0.0452(0.0122)				

Table S2. Comparison of Csp values of various Co-MOF materials.

MOFs	F g^{-1}/ mVs^{-1}	F g^{-1}/ A g^{-1}	F g^{-1}/A g^{-1}	Refs.
$[Co_2(OH)_2C_8H_4O_4]$		2564/1	1165/20	42
Co8-MOF-5	3.27/25	1.98/0.01		43
Co-BDC	131.8/10			44
Co-NDC	147.3/10			44
Co-BPDC	179.2/10			44
Co-LBDC		230.5/0.5		45
Co-LMOF		1786/1	592/20	46

Table S3. Crystal data and structural refinement parameters for compounds **1**–**3**.

	1	**2**	**3**
formula	$C_{138}H_{128}Co_6N_{12}O_{34}S_{36}$	$C_{64}H_{46}Co_5N_4O_{18}S_{24}$	$C_{22}H_{24}CoN_2O_7S_6$
fw	4006.5	2223.3	679.8
cryst size (mm^3)	0.04×0.08×0.30	0.13×0.15×0.55	0.05×0.07×0.10
cryst syst	monoclinic	triclinic	monoclinic
space group	$P2_1/c$	$P\bar{1}$	$P2_1/c$
a (Å)	11.6564(13)	7.4395(15)	16.045(4)
b (Å)	29.388(3)	17.175(3)	8.4992(17)
c (Å)	47.199(6)	17.822(4)	25.844(5)
α (deg)	90	91.19(3)	90
β (deg)	92.119(3)	96.90(3)	124.895(11)
γ (deg)	90	93.44(3)	90
V ($Å^3$)	16157(3)	2255.7(8)	2890.7(11)
Z	4	1	4
ρ_{calcd} ($g\ cm^{-3}$)	1.639	1.635	1.553
F(000)	8128	1119	1380
μ (mm^{-1})	1.144	1.518	1.070
T (K)	223(2)	223(2)	223(2)
reflns collected	235249	21662	26583
unique reflns	28236	11127	6609
observed reflns	18826	10137	5551
no. params	2063	6125	353
GOF on F^2	1.174	1.018	1.171
R_1 [I>2σ(I)]	0.0929	0.0982	0.0794
${}_wR_2$ [I>2σ(I)]	0.1744	0.1596	0.1771

4. Equations

$$C_{sp} = \frac{\int_{V_0}^{V} I(V)dV}{mv(V - V_0)} \quad (1)^1$$

where C_{sp} (F g^{-1}), m (g), v (V s^{-1}), ($V^{-}V_0$), and I(V) are the specific capacitance, mass of the active material, potential scan rate, potential range and current density, respectively.

$$C'_{sp} = \frac{I \times \Delta t}{\Delta V \times m} \quad (2)^1$$

where C_{sp}' (F g^{-1}) is the discharge specific capacitance, I is the discharge current (A), Δt is the discharge time (s), ΔV is the potential window, and m is the mass (g) of the active material.

References

1. Lu, M.; Yuan, X.-P.; Guana, X.-H.; Wang, G.-S. Synthesis of nickel chalcogenide hollow spheres using an L-cysteine-assisted hydrothermal process for efficient supercapacitor electrodes. *J. Mater. Chem. A* **2017**, *5*, 3621–3627.